

Running Head: *Grain Size Parameters for Floating Grains*

CRITICAL GRAIN SIZE PARAMETERS FOR PREDICTING FRAMEWORK AND “FLOATING” GRAINS IN SEDIMENTS

STEVEN L. BRYANT¹, CHRIS LERCH² AND MICHAEL E. GLINSKY²

¹ Dept. of Petroleum and Geosystems Engineering, The University of Texas at Austin, Austin, TX, USA
78712-0228

² BHP Billiton Petroleum, 1360 Post Oak Blvd., Houston, TX, USA 77056-3020

Keywords: grain size distribution; floating grain; acoustic velocity; porosity;
permeability; mixture; fines

ABSTRACT

In unconsolidated sediments, some grains form a load-bearing framework while others may “float,” that is, occupy volume without contributing to mechanical strength. The latter grains affect the relationship between acoustic velocity and porosity as well as the permeability of the sediment. We propose that characteristic features of the grain size distribution are indicators of the fraction of floating grains. The criterion for “floating” involves grain-scale geometry not accessible from macroscopic models of grain packing, so we support this proposition with an examination of computer-generated model sediments (dense, disordered packings of spheres) having two sizes of spheres. The analysis reveals two thresholds. First, the fraction of floating grains is larger when the volume fraction of small grains is below ~40%. In packings satisfying the first threshold, a second threshold exists: if the large grain radius is sufficiently greater than the small grain radius (by a factor of 3, or half a decade on a logarithmic scale), the fraction of floating grains is significantly larger. These thresholds are qualitatively consistent with

field observations of anomalously slow P-wave velocities in several poorly to semi-consolidated reservoirs. The grain size distributions in these reservoirs are sufficiently broad to satisfy the two thresholds, and the emergence of a second mode in the distribution correlates with greater anomaly in the velocity-porosity trend. The maximum fraction of floating grains in the model sediments is comparable to the value needed to explain the anomaly quantitatively. Significantly, the thresholds for floating grains are closely related to those known to affect trends of macroscopic properties of sediments (porosity, permeability). The grain-scale model may thus serve more generally as a microstructural complement to established macroscopic models.

INTRODUCTION

The relationship between acoustic compressional velocity (V_p) and porosity (ϕ) of a sediment or a sedimentary rock is fundamental to hydrocarbon exploration employing seismic methodologies. Predictive relationships are particularly valuable because they provide an independent constraint on the inversion and interpretation of seismic data. But the scarcity of such relationships means that most practical work is based on empirical correlations.

An example of this is shown in Figure 1, which plots bulk density against P-wave velocity. The dotted line is the average behavior of sand reservoirs in a petroleum exploration province. The trends labeled I, II and III are from reservoirs in the same province. Trend I is typical of the average reservoir. Trend II deviates significantly from the average behavior, and trend III deviates still more. The deviation cannot be attributed

to variations in density or elastic moduli of the grains composing the sediment (DeMartini and Glinsky, 2006). The simplest explanation is that part of the rock volume consists of “floating” grains. These grains occupy space and thus increase rock density (reduce porosity) but are not part of the rigid, load-bearing framework of grains. Because the transmission of a sound wave is predominantly through this framework, floating grains do not affect acoustic velocities. Consequently, a sediment containing floating grains would exhibit higher bulk density and lower porosity than a sediment having the same acoustic velocity and mineralogy but with no floating grains. This explanation has important implications. For example, interpreting measurements without considering the floating grain phenomenon will lead to overestimates of porosity.

While floating grains offer an elegant explanation of the density anomaly in Figure 1, their existence in materials that can sustain a load through a network of grain contacts may seem counterintuitive. Indeed, the motivation of the work reported here is to seek independent evidence for floating grains.

An important first step is to consider the influence of grain packing. The simplest possible analogue to natural sediments is a packing of spheres. Equal spheres can be packed regularly into hexagonal, simple cubic, or face-centered cubic arrangements (see Fig. 2). Regular packings have no floating grains. All grains are part of the framework. No grain can move while others remain fixed.

In contrast, dense disordered packings (or, more precisely, maximally jammed packings) of equal spheres invariably contain “rattlers” (Kansal et al., 2002) or “floating” grains (Thane, 2006). These grains touch several other framework grains but are free to

move in at least one direction (see Fig. 2.) The framework grains are jammed by their contacts with other framework grains and cannot move in any direction. Consequently framework grains cannot be rearranged locally to eliminate the freedom of movement of any of the floating grains.

We propose that a similar mechanism applies to natural sediments. Floating grains occur because a load-bearing, maximally jammed framework of grain contacts emerges before all the grains get incorporated into the framework.

Our study uses computer-generated sphere packings, but the floating grains are not artifacts of the algorithms employed. That is, it is not possible to eliminate floating grains by continued iteration or by modification of the algorithm. The reason is that small, rigid structures, consisting of several grains in mutual contact, form as the packing becomes denser. When the structures contain only a few grains it is possible to rearrange them to pack tightly around a floating grain. As the size of the rigid structures increases, it becomes correspondingly more difficult to rearrange the grains relative to each other. A floating grain inside such a structure will therefore remain so, even as the packing density increases. Observations confirm this expectation. For example, in the best-characterized monodisperse experimental random sphere packing (Finney, 1970) approximately every hundredth sphere in the packing is floating (see analysis below and Thane, 2006). Floating grains should be therefore regarded as inherent in disordered packings, one of the features distinguishing them from regular packings.

We are thus led to expect the existence of floating grains in monodisperse unconsolidated sands. Naturally occurring sediments are not perfectly sorted, however,

and we must consider the possibility that grains with a distribution of sizes might fit together more snugly than monodisperse grains. This would reduce or eliminate the occurrence of floating grains. Examination of the grain-size distributions shown in Figure 3, confirms this possibility. The velocity-density trend of Reservoir I is not anomalous; it is typical of other reservoirs in the province. Its grain-size distribution is broad, but it has a small proportion of small grains relative to large grains. Evidently this proportion does not lead to enough floating grains to affect velocity. Further examination also suggests another hypothesis. Reservoir II shows a somewhat larger proportion of small grains relative to large grains than Reservoir I. Reservoir III shows a still larger proportion; in fact, a second mode of small sizes is present. The progression from Reservoir I to Reservoir III suggests that the velocity/density anomaly emerges, then strengthens, as certain characteristics of the grain-size distribution vary. This observation motivates the following hypothesis:

If small grains in a sediment are appropriately numerous and sufficiently small, many of them "float", i.e. they are not captured by the framework grains during deposition and burial.

This floating fraction increases density without contributing to stiffness of the sediment.

The preceding hypothesis was motivated by the observations of Figs. 1 and 3, but similar thresholds or critical values have long been studied in bidisperse (and polydisperse) packings (e.g. Furnas, 1929; Yerazunis et al., 1965; Clarke, 1979; Shakoor and Cook, 1990; Koltermann and Gorelick, 1995; Kamann et al., 2007). Consider, for

example, that the porosity of a packing of small grains decreases as large grains are mixed in. The porosity of a packing of large grains also decreases as small grains are mixed in. It follows that the porosity of a mixture of small and large grains must exhibit a minimum at a critical volume fraction of small grains. The critical volume fraction is associated with the transition from a matrix of large grains, in which small grains fill voids between large grains, to a matrix of small grains in which large grains are embedded. Similarly, the permeability of a mixture decreases rapidly as the volume fraction of small grains increases from zero to the critical volume fraction, but changes slowly for volume fractions exceeding the critical value.

This behavior is well established experimentally, and several models for it have been advanced. The models relate macroscopic properties (porosity, permeability) to average mixture properties (ratio of large grain radius to small grain radius, volume fraction of small grains) and empirical parameters (e.g., the minimum value of porosity and the maximum volume fraction of small grains in voids of large grains (Koltermann and Gorelick, 1995)). The concept of "fractional packing" (Koltermann and Gorelick, 1995; Kamann et al., 2007) corrects the rather severe underestimation of the minimum porosity by the "ideal packing" model. This is an important indication that a grain pack near the critical volume fraction must have complex grain-scale structure. Our computer-generated model sediments provide quantitative insight into this structure. We will argue that floating grains are one manifestation of this complexity.

Properties of bidisperse packings are also known to depend on the ratio of grain sizes (large grain radius to small grain radius; we refer to this as the *radius ratio* or RR).

For small volume fractions of small grains, this is a consequence of whether the small grains can fit into voids between densely packed large grains. Thus the value of minimum porosity depends upon RR. The extended fractional packing theory of Kamann et al. (2007) depends on RR implicitly (through the minimum porosity and the use of pre-mixed sediment volumes to determine volume fractions) but can be applied without otherwise accounting for whether small grains fit in voids. We will see that the grain-scale structure of a packing varies with RR more dramatically than do macroscopic properties, and as a consequence the threshold RR for floating grains is sharper.

We organize this paper as a test of the above-hypothesized existence of thresholds for floating grains. The key feature of the grain-size distribution is the presence of grains sufficiently small compared to the large grains. We idealize this situation with a two-size population of grains. We consider a modest range of ratios of grain sizes and the full range of volume fractions of small grains, anticipating that the fraction of floating grains will be sensitive to these parameters. We further idealize the grains as spheres and employ an isotropic numerical scheme for generating dense, disordered sphere packings. The latter idealizations are convenient but not crucial. Distinguishing grain contacts from not-quite-contacts is feasible in computer-generated sphere packs but remains a formidable challenge even in high resolution 3D digital images of sediments (Arns et al., 2005; Thompson et al., 2006). Similarly, testing a grain for freedom of movement is a great deal simpler with spheres than with real grain shapes. Our experience with this type of idealization teaches that if the phenomenon of interest is found in the idealized system, then it is worthwhile to search for it in more realistic sediments. Conversely, if floating

grains prove not be a significant feature in these two-size sphere packs, then the occurrence of floating grains in natural sediments would have to be the consequence of mechanisms not considered in our model. We compute one macroscopic property of the model sediments, porosity, to validate the packing algorithm. Our primary purposes are first to describe an approach for determining the grain-scale structure of packings, which is not accessible from existing macroscopic packing models, and then to apply it to the problem of floating grains.

METHODS

The use of dense, disordered, sphere packs as model sediments, and of geometrically modified sphere packs as models of clastic rocks, is now well established (Bryant et al, 1993; Bryant and Raikes, 1995; Bakke and Øren, 1997; Øren et al., 1998; Jin et al., 2003). Many properties of practical interest depend strongly upon how grain space and void space are arranged. Dense disordered packings capture several key characteristics of grain-scale geometry in naturally occurring materials (Bryant et al., 1993, 1996), and consequently the grain shape is not crucial for some applications. Of relevance here is the prior use of this approach to predict acoustic velocities (Bryant and Raikes, 1995) and stress-strain behavior (Jin et al., 2003; Park et al., 2007, 2006) in sandstones. Because the packings are completely characterized geometrically by knowledge of the sphere centers and radii, it is possible to make *a priori* predictions of macroscopic properties that depend on geometry. This capability is important, for it eliminates the possibility of adjusting grain-scale parameters to fit measurements. Thus

successful predictions provide confidence in the model. Failures are also valuable, because they indicate that the model does not include a key physical phenomenon. Nevertheless the prediction of macroscopic properties is only of secondary interest in this work. Our focus is upon a microscopic property (existence of floating grains) with macroscopic consequences (velocity anomaly).

Packing Algorithm

The cooperative rearrangement algorithm was used to create the sphere packings in this study. In our implementation, the algorithm yields packing fractions between 0.637 and 0.649 for monodisperse spheres, a range consistent with experimental packings, such as the Finney packing (Clarke and Wiley, 1987). The cooperative rearrangement algorithm consists of three steps: (1) initial point generation, (2) sphere growth, and (3) overlap check and removal. Steps (2) and (3) are repeated until a dense packing is obtained.

The first step in the algorithm involves assigning randomly generated positions to nominally zero-radius spheres (Fig. 4a). A user-specified fraction of points is randomly chosen to become small spheres. The user also specifies the radius ratio (RR) of large to small spheres in the bidisperse mode. The packings used here were created within a cubic computational domain. The domain is periodic, meaning that a sphere whose surface extends beyond one face of the cube “wraps around” to enter the opposite face. This stratagem eliminates edge effects, notably the packing order imposed by the presence of any smooth wall.

In the second step of the process, the spheres are grown so that they fill more of the domain (Fig. 4b). Growth occurs by incrementing all sphere radii simultaneously. The increment for small spheres is adjusted to preserve the user-specified radius ratio. Relatively large increments are possible when spheres are small, but as the packing density increases much smaller increments are necessary. Thus we adjust the increment dynamically during the simulation.

Cooperative rearrangement occurs in the third step of the process (Fig. 4c). In general the size change in step 2 results in overlapping spheres. In our application overlap is physically forbidden (see Thane [2006] and Mousavi and Bryant [2007] for applications in which overlap is admissible). Therefore, all spheres are checked after each size change to determine whether they overlap their neighbors. Once an overlap is found between a pair of spheres, it is removed by pulling the spheres apart along the axis joining their centers until the spheres are in point contact. This displacement may itself cause new overlaps. Thus overlap removal is an iterative process. After an increment in size, we loop over all spheres carrying out displacements of centers until no overlaps remain.

Steps (2) and (3) are iterated until the packing is maximally dense. The end state is found as follows. If after an increment in size some overlaps cannot be removed after a large number ($\sim 10^4$) of iterations, then the spheres must be reduced in size. A small decrement is chosen to allow the overlaps in the packing to be resolved. The algorithm ends at a densely packed, disordered, overlap-free state. Figure 5 illustrates the result of applying this algorithm to a small set of 100 equal spheres.

Floating Grains

A subroutine was created that finds floating grains within a maximally dense packing produced by the cooperative rearrangement algorithm. The subroutine requires the user to define “floating” in terms of the minimum distance that a sphere can move without encountering another sphere. The minimum distance is arbitrary and may depend on the specific application. For example, if the approximate distance of grain movement as a pressure wave passes is known, the definition of a floating grain may include any grain that can move farther than that distance. We discuss the threshold used in this work below.

After setting the threshold of travel we carry out a series of test displacements for each sphere in a packing. A displacement moves the center of the test sphere by the threshold travel distance in a specified direction. After each displacement, the test sphere is checked in its new position to determine whether overlaps were created with nearby spheres. Figure 6 illustrates the concept. If the test movement creates no overlap with neighboring spheres, it is considered to be a floating grain.

If the movement creates overlaps with nearby spheres, the sphere cannot be described as floating with respect to that particular direction. However, it is possible that the grain may be able to move in another direction. In this work, a dense uniform mesh of 625 points was placed on the surface of the test sphere. The test directions are rays from the sphere center through each mesh point.

In our model, floating grains affect acoustic velocity simply by occupying space. Thus the relevant parameter is the volume fraction of floating grains, which we obtain by

summing the volumes of all grains identified as floating, then dividing by the volume of all grains.

Capture Fraction

The volume fraction of floating grains directly affects the velocity/density trend, but the concept of a capture fraction provides more insight into the mechanism leading to floating grains. The capture fraction is the fraction of candidate floating grains that are captured as part of the framework or matrix and thus are mechanically locked in place. Both large and small grains are candidates for floating grains, but in practice almost all the large grains are captured. In contrast the capture fraction of smaller grains varies widely, depending on the volume fraction of small grains and on the radius ratio.

RESULTS AND DISCUSSION

Basic Statistics

To validate the packing algorithm, statistics for monodispersed packings were compared against Finney pack statistics. The latter were computed from the measured spatial coordinates of sphere centers (Finney, 1970). Measured statistics for monodispersed packings are the radial distribution function, porosity, and the number of floating grains in the packing. For bi-dispersed packings, porosity, coordination numbers, and pore throat distributions were calculated. The porosities of bi-dispersed packings are compared below with experiments reported in the literature.

Monodisperse Packings.---The Radial Distribution Function (RDF) is one measure of the order or structure of a granular material. The RDF of a particular packing

is derived from counting the number of spheres N that are separated from a given sphere by a distance in the interval $[r, r+dr]$. The separation r between two spheres is the distance between their centers. In a monodisperse packing the minimum separation is $2R$, where R is the radius of the spheres. At large separation (large r) the number density of the spheres found within the spherical shell of thickness dr approaches the average number density of spheres in the packing, ρ_0 . If the packing has porosity ϕ , then

$\rho_0 = \frac{3}{4\pi R^3}(1-\phi)$. It is convenient to normalize the RDF by ρ_0 , so that at large r the

value of the RDF approaches 1 for any mono-dispersed packing. The RDF for a crystalline material or a regular packing of spheres shows a series of sharp, narrow peaks that correspond to various multiples of the lattice spacing. At the other extreme, the RDF of a randomly distributed collection of points in space shows fluctuations about the mean density but no organized peaks nor valleys. A dense disordered packing of equal spheres is obviously not perfectly ordered, but as discussed below it is not completely random either, because of the requirement that spheres cannot overlap. Thus its RDF is intermediate between the two extremes.

Figure 7 shows that the computer-generated packing closely matches the RDF of the Finney packing. The shell thickness dr , in this study, is about 1% of a sphere's radius. The RDF in Figure 7 is dominated by a large peak (off the scale of the y axis) at separation $r = 2R$. This separation corresponds to pairs of spheres in point contact. Many such contacts are expected in a dense packing (see below), so this peak is not surprising. Of more interest are the smaller peaks at $r = 2\sqrt{3}R$ (r_{AB} in Fig. 7) and $r = 4R$ (r_{AC} in

Fig. 7). The former corresponds to an arrangement of four spheres in the same plane in two adjacent equilateral triangles. The latter corresponds to three spheres in contact along a straight line. The peaks in the RDF indicate that these arrangements are relatively common. Conversely the valleys in the intervals $2.2 < r/R < 3.2$ and $4 < r/R < 5$ indicate that it is relatively rare to find spheres separated by those distances in a dense disordered packing. Significant peaks and valleys do not persist at separations greater than about $6R$. Thus dense disordered packings exhibit short-range order (arrangements of two, three and four spheres in contact), but no structure that is perceptible at the scale of tens of grains or larger.

The Finney pack porosity is 0.36; applying the cooperative rearrangement algorithm to sets of 10^3 to 10^4 equal spheres, we obtain porosities of 0.359 ± 0.002 . The average coordination number (number of sphere contacts per sphere, Z) of these packings is 5.61 ± 0.03 . This agrees well with the value found for the Finney Pack ($Z = 5.61$). To calculate the latter, two spheres were considered to be in contact if the gap between them was less than $0.01 R$. The larger tolerance is necessary since the data had a larger error than the simulations (Mellor, 1989).

Bi-dispersed Packings.---The bi-dispersed packings are characterized by two parameters: the value of RR (ratio of large sphere radius r_l to small sphere radius r_s) and the volume fraction of small spheres VF . For our purposes a convenient definition of VF is the ratio of solid volume of the small spheres to the total solid volume, i.e. $VF = N_s r_s^3 / (N_s r_s^3 + N_l r_l^3)$, where N_s and N_l are the numbers of small and large spheres, respectively. Figure 8 shows the porosities of bi-dispersed packings with different values

of RR as a function of VF. Error bars for the packings with RR = 5 grow as the volume fraction of small spheres increases from 0 to 0.4. This is because the number of spheres needed to obtain reliable statistics became computationally prohibitive. Packings for RR = 4 and RR = 5 used 5000 to 40000 spheres. Packings for smaller radius ratios used 5000 spheres. As VF, the fraction of solid volume composed of small spheres, increases from zero, the porosity decreases to a minimum, then increases to the monodisperse limit of 0.36. As RR increases, the minimum porosity decreases. The minimum porosity is much smaller when radius ratio RR is three or greater. The trend of porosity vs volume fraction small spheres is asymmetric. This is a manifestation of the capability of sufficiently small spheres to fit between larger spheres without disrupting the framework of a large-grain matrix. The packings exhibit a minimum in porosity in the vicinity of VF = 30%.

The porosity trends for several values of RR are compared in Figure 9 with data for sand-clay mixtures (RR \gg 1) under a confining pressure of 20 MPa (Koltermann and Gorelick, 1995), for binary sphere packings (Yerazunis et al., 1965), for binary mixtures of broken solids (Furnas, 1929) and for mixtures of sand (Kamann et al., 2007). The model is qualitatively consistent with the measurements. For example, increasing RR causes a smaller minimum porosity, and the minimum occurs at VF in the range of 20% to 40%. Figure 9a also shows quantitative agreement between our packings and the results of a different sphere packing algorithm (Clarke and Wiley, 1987).

The trends in Figs. 8 and 9 are familiar, and as noted above, macroscopic mixing theories exist which account for these trends. The computer-generated packings are not intended to supplant these theories but to provide grain-scale information to complement

those theories. Floating grains are the focus of this work, but insight into other grain-scale features is also available. For example, there is a notable decrease in the minimum porosity of the computer-generated packings when the radius ratio increases to 3 from 2. The reason is that when RR is 2 or less, the smaller spheres are primarily “replacement” spheres. That is, they occupy a place where a large sphere would otherwise have been in a mono-dispersed packing. As the radius ratio increases, the small spheres can fit into more of the pores between large spheres. They can thus act as “pore filling” spheres rather than replacement spheres.

The distinction between replacement and pore-filling spheres suggests that a threshold value of RR will be useful in interpreting these results. For example, Kamann et al. (2007) associated this threshold with the size of a pore in a simple cubic packing of larger grains. This notion can be made more precise by considering the pore body sizes in a monodisperse dense packing, as shown in Figure 10. For these purposes the radius of a pore body is defined as the radius of the largest sphere that can be inscribed within the pore. Pore bodies are here defined as the volume within groups of nearest-neighbor spheres, as determined by a Delaunay tessellation of the sphere centers (see next section, and Bryant et al., 1993; Mason and Mellor, 1995). The reason the threshold RR is between 2 and 3 becomes evident upon examination of the distribution of pore body sizes. Only 10% of the pores in a monodisperse packing can accommodate small spheres when $RR = 2$. Thus almost all the small spheres in a bidisperse packing with $RR = 2$ must be replacement spheres; it is simply not possible to fit them in the voids between densely packed large spheres. In contrast, for $RR = 3$ a small sphere can be placed within 70% of

the pores in a dense packing of larger spheres. Of course neither sediments nor our computer-generated packings are constructed by sequentially placing grains in order of size. The point is that a threshold value of RR exists, below which the small spheres must be replacement spheres and above which the small spheres may be either replacement or pore-filling.

A second threshold is implicit in this analysis. Clearly there are a finite number of pores per unit volume in a monodisperse packing. This places an upper bound on the number of pore-filling spheres. Thus if VF is sufficiently large, some small spheres must become replacement spheres, regardless of the value of RR. If VF is significantly larger than this threshold, it becomes natural to change perspective, and to regard the large spheres as inclusions within a matrix of small spheres. We will elaborate on these thresholds in the context of floating grains in the next section. A qualitative illustration of these thresholds appears in Figure 11, a series of 2D slices taken from packings with RR values of 1.5, 2, 3, and 4 for small sphere volume fractions VF of 5%, 40%, and 80%. The value of RR is constant in a row of Fig. 11, and increases from top to bottom. The value of VF is constant in a column and increases from left to right. The transition of small grains from replacement to pore-filling as RR increases is apparent in the left column of images. The transition from large-grain-dominated matrix to small-grain-dominated matrix as VF increases is apparent from left to right in any row of the images.

Pore throat size distributions. Because the locations of all spheres are known, it is possible to identify pore throats unambiguously using Delaunay tessellation. Applied to centers of spheres, the tessellation finds groups of four nearest neighbor spheres. (Four

spheres are "nearest neighbors" if no other sphere center lies inside the group's "circumsphere". The circumsphere is the unique, hypothetical sphere on whose surface all four sphere centers lie.) The void area between any three spheres in a group is therefore a local minimum. This area naturally corresponds to a pore throat. A convenient measure of the size of a throat is the radius of a circle inscribed between the spheres defining the throat. When RR is large, this measure frequently yields unrealistically large values for throats involving two small grains. Thane (2006) introduced a correction for this situation that accounts for the presence of the largest nearby sphere. In a dense packing, the nearby sphere always restricts the void area near the throat, and requiring the inscribed circle not to overlap the nearby sphere always yields more representative throat sizes.

The pore throat size distributions (PTSDs) obtained in this fashion are shown for a range of VF and RR values in Fig. 12. Each PTSD is plotted together with a reference PTSD obtained from the sphere center coordinates in a monodisperse packing measured by Finney (1970). Thus the PTSD shifts toward smaller throats as VF increases or as RR increases. In all plots, the throat radius is normalized by the radius of the larger sphere in the packing. The reference PTSD shows a characteristic peak at about $r_{throat}/R = 0.15$. This is the throat formed by three touching equal spheres.

The transition from large-grain-dominated matrix to small-grain-dominated matrix is apparent in the columns of Fig. 12. In any column, the top row (VF = 0.05) shows that many of the throats in the reference monodisperse packing are still present in the bidisperse packing, indicating that the large grains are forming the matrix. Some "new" throats (dimensionless radius smaller than 0.15) occur in the bidisperse packing,

the consequence of one small grain and two large grains forming a throat. Moving down a column, the throats formed by three large grains become increasingly rare, and throats involving two or three small grains become more common. At $VF = 0.4$ (third row), the small grains are beginning to comprise the matrix, especially for larger RR . The peak throat radii corresponding to two small and one large, or to three small grains in contact are clear, and increasing VF to 0.8 does not shift this peak significantly.

Moving left to right along the first or second row of Fig. 12, we see the threshold RR at which small grains become pore-filling, rather than replacement grains. At $VF = 0.05$ and $RR = 1.5$, the small grains cause only a minor shift in the PTSD. This is because when a large grain is replaced by a grain two-thirds its size, the throat radius is only slightly smaller. But at $VF = 0.05$ and $RR = 3$, a small grain can fit within the pore of a matrix of large grains. A pore-filling small grain forms a large number (locally) of smaller throats. Consequently the PTSD shifts noticeably to the left relative to the reference. The same effect accounts for the greater shift in PTSD with RR when $VF = 0.20$ (second row). However at sufficiently large VF , the grains are part of the matrix regardless of RR . Thus the third and fourth rows ($VF = 0.4$ and 0.8 , respectively) show a significant peak at smaller throat sizes for all RR .

We consider the implications of these changes in PTSD for permeability in the Discussion.

FLOATING GRAINS

Effect of Threshold Displacement Distance.---Different values of the minimum distance of unhindered movement that would constitute a floating grain were tested. For each choice of minimum distance, the volume percent of floating grains was calculated.

The minimum distance of unhindered movement varied from 0.01 to 0.5 of the radius of the tested sphere. Three packing sizes were tested: 6000, 7000 and 9000 spheres. As the results in Figure 13 for a monodisperse packing indicate, few grains would be considered floating if the threshold displacement were larger than $0.3 R$. The trends in Figure 13 suggest that it is reasonable to regard 3% as an upper limit on the fraction of floating grains in monodisperse packings. This is consistent with the findings of Kansal et al. (2002). Because some scatter is evident in the floating fraction when the minimum displacement is $0.01 R$, we elect to use $0.1 R$ as the threshold displacement for a floating grain. The volume fraction of grains meeting this criterion is a little more than 0.5%.

The choice of threshold is not crucial to the findings presented below. We anticipate that conclusions regarding the occurrence of floating grains will not change *qualitatively* as the threshold displacement varies in the range of $0.01 R$ to $0.1 R$. That is, if a strong correlation between the fraction of floating grains and the grain size distribution is found using a convenient value of threshold in this range, the correlation is expected to hold if a different threshold value is used.

Effect of Bidisperse Packing Parameters on Floating Grain Fraction.---The volume percent of floating grains in the two-size packings with values of RR of 1.5, 2, 3, and 4 are shown in Figure 14. For large RR, the floating grain fraction exhibits a peak

around $VF = 0.2$. The peak becomes less pronounced and shifts to larger fractions of small grains as RR decreases. As VF increases beyond 0.4 the floating grain fraction becomes independent of RR . Moreover the floating grain fraction within the packings for all radius ratios approaches 0.5%, the value characteristic of a mono-dispersed pack. As suggested by Figure 11, at large VF , the load-bearing framework consists of small grains with occasional large grain inclusions. None of the large grains are floating in this case. The framework of small grains would therefore be expected to have similar characteristics to a monodisperse packing, in particular, the same inherent fraction of floating grains.

Figure 14 shows that a small fraction of floating grains always exists, even in monodisperse packs ($VF = 0$ or $VF = 1$). Thus we associate the velocity anomaly not with the existence of floating grains, but with a sufficiently large volume fraction of floating grains. In our bidisperse packings, large values of floating grain fraction occur over a relatively narrow range of values of VF , between 0.1 and 0.3. This is a consequence of the role of small grains changing from void-filling to load-bearing, becoming part of the matrix at about $VF = 0.4$. If there are many small grains, they tend to be an integral part of the load-bearing framework. Figure 15 illustrates this concept in a typical pore body in a packing of $RR = 5$ containing 40% by volume small spheres. If there are too few small grains ($VF < 0.1$), many of them will be floating, but the fraction of floating grains is not large because the fraction of small grains is small to begin with. Thus it is not just the width of the grain size distribution that determines the prevalence of floating grains; the frequencies must also be appropriate.

The other salient feature of Figure 14 is the effect of RR. The maximum fraction of floating grains is much larger if the radius ratio is larger than a threshold value. The threshold lies between 2 and 3 for these two-size packings. At $RR = 2$, the maximum floating grain fraction is less than 4%. When $RR = 3$ or 4, the maximum floating grain fraction is more than 8%. This suggests a second key characteristic of a grain size distribution that exhibits floating grains: if the small grains are sufficiently small, the peak fraction of floating grains is much larger.

As floating grain fraction increases, the porosity decreases in these model sediments, as shown in Figure 16. However, the crossplot shows two trends. This is because the small porosities occur over a relatively wide range of volume fractions of small grains (Fig. 8), whereas large floating grain fractions occur over a relatively narrow range. Thus porosity alone is not a reliable indicator of the volume fraction of floating grains. For the same reason, floating grains confound the correlation between porosity and permeability (DeMartini and Glinsky, 2006).

Extension to Natural Poorly- to Semi-consolidated Sediments.---The message of Figure 14, and of this paper, is that a substantially larger volume fraction of floating grains can occur in a model sediment (a dense, disordered packing of spheres of two sizes) if two conditions are satisfied: there are neither too many nor too few small grains, and the small grains are at least a factor of 3 smaller than the large grains. The extension of this conclusion to natural sediments can be stated as follows: if a grain size distribution shows two sufficiently separated modes (at least half a decade on a logarithmic scale) and

the mode at smaller sizes is not too pronounced, then that sediment will exhibit a much larger fraction of floating grains.

This hypothesis is quantitatively satisfied by the measurements in Figures 1 and 3. The density anomaly occurs for sediments whose grain size distribution is skewed toward small sizes, and the shift in density increases as the frequency of small grains increases. Moreover, the magnitude of the volume fraction of floating grains (between 1% and 10% of the solid volume) is the same as the magnitude needed to explain the density anomaly of Figure 1 (DeMartini and Glinsky, 2006).

The thresholds of VF and RR associated with floating grains are closely related to critical values of VF and RR associated with macroscopic properties (porosity, permeability). We elaborate upon this point in the Discussion.

Capture Fraction.---The preceding analysis implies that the capture fraction of small grains should likewise show a pronounced dependence on RR when VF is less than 40%. The trends shown in Figure 17 bear out this expectation. If VF exceeds 40%, almost all the small grains are captured, regardless of size. This is because the small grains are so numerous that they cannot be accommodated only in the voids between load-bearing large grains. Thus they must disrupt the arrangement of large grains and form part of the load-bearing framework. In contrast, for VF less than 40% the packings exhibit smaller capture fractions. The capture fractions are much smaller but not strongly dependent on RR when the large grains are three or more times larger than the small grains. As for the minimum in porosity discussed above, this behavior is analogous to a phase transition occurring when the small spheres can fit into the voids within a framework of large

grains. The capture fraction is small for all values of RR except RR=1.5 when VF is less than 10%, but as shown in Figure 14, the floating fraction is still small because the volume fraction is small. The small spheres in packings of a radius ratio of 1.5 replace the larger spheres in the load-bearing framework, because they are too large to fit into the pores in a framework of larger spheres.

DISCUSSION

Relationship to permeability variation.---Kamann et al. (2007) report that the permeability of bidisperse mixtures decreases as VF increases from 0 to 0.4. For $VF > 0.4$, the permeability is roughly constant. (Similar behavior occurs in the model of Koltermann and Gorelick (1995).) This permeability trend is consistent with the trends in pore throat size distributions in Fig. 12. For small VF, a small change in VF produces a large change in the PTSD. The change is primarily an increase in the proportion of small throats. For larger RR the fraction of large throats also decreases. Both changes cause the permeability to decrease. For $VF > 0.4$, even a large change in VF does not alter the PTSD substantially. This is consistent with the small grains dominating the framework in this range of VF. That is, for any value of VF exceeding 0.4, nearly all the throats involve two or three small grains. The large grains act as embedded inclusions and therefore have little effect on the PTSD. The lack of variation in PTSD in this range of VF is consistent with the insensitivity of permeability in the same range.

Relationship to multiphase flow properties.---The arrangement of two immiscible fluids in the pore space depends strongly upon the geometry of the pore space.

The variations in PTSD described above should therefore cause the capillary pressure curves to change substantially for VF between 0 and 0.4. For packings with $VF > 0.4$, the capillary pressure curves should be similar to the curve measured in a small-grain-only packing. Analogous trends would be expected for other macroscopic properties that depend on pore-scale fluid configuration such as relative permeability and electrical resistivity. The occurrence of the floating grain velocity/density anomaly would therefore be correlated with sensitivity or substantial variability of other macroscopic properties to relatively small changes in the fraction of small grains.

Extension of grain-scale microstructure model.---The methodology described in this paper can be extended to other factors influencing grain packing. An example is the deformation of ductile grains during burial. A simple geometric model of the effect of deformation is the penetrable sphere (Thane, 2006; Mousavi and Bryant, 2007). In this model a sphere can have a soft outer shell surrounding a hard, impenetrable core. If the soft shell is penetrated by a hard grain, the radius of the penetrated sphere is increased so that the non-overlapping volume of the sphere remains constant. The predicted trend of porosity as a function of ductile grain fraction is consistent with measurements (Mousavi and Bryant, 2007). If the ductile grains tend to be a different size than the other grains, then it is possible that their deformation would overprint the floating grain trends found in hard-sphere packings shown above.

Modeling the effect of grain shape and roughness is difficult and is computationally intensive. Given that the broad trends observed in sand mixtures are consistent with the very simple models described here, a more productive extension of

the approach might be to different grain size distributions. As high resolution X-ray computed tomography becomes increasingly powerful (resolution approaching one micron) and more widely available, direct observation of floating grains within a sediment should be feasible. This would offer a powerful validation of the grain-scale predictions made here.

Thresholds and Phase Transition.---The range of parameter space [RR, VF] described above is not exhaustive, but it is sufficient to demonstrate the existence of important thresholds for the floating-grain phenomenon. These thresholds are closely related to previously established thresholds for macroscopic properties. Thus it is useful to summarize the behavior in terms of a phase diagram like that of Figure 18. In dense, disordered packings of two sizes of spheres, the minimum porosity, the volume fraction of floating grains, and the capture fracture all display different behavior in the vicinity of critical values of RR and VF. As shown in Fig. 18, three regions of parameter space can be identified relative to these critical values.

There exists a threshold or critical value of the volume fraction of small grains, VF_c , above which the small grains comprise much of the load-bearing matrix. This is true regardless of the value of RR. In this region of parameter space (upper portion of Fig. 18) the sediment has few floating grains. Large grains can be regarded as inclusions within a matrix of small grains. Such sediments should follow typical density-velocity trends. As VF increases, porosity increases while permeability changes slowly or remains roughly constant.

Below the threshold VF_c , two types of sediment are possible, depending on RR. Below the critical radius ratio RR_c (lower-left region in Fig. 18), both small and large grains are integrated into the load-bearing matrix. In contrast to packings above VF_c , here the large grains dominate the matrix. Nevertheless the small spheres act as replacement grains, and few floating grains occur. Thus typical density-velocity trends should apply to sediments in this range of parameter space. As VF increases, porosity and permeability both decrease, though not rapidly.

When RR exceeds RR_c , the small spheres can act as pore-filling grains. This leads to a type of phase transition, from replacement grains to arrangements of pore-filling small grains. Pore-filling grains *may* play a role in establishing a rigid, load-bearing framework, but they are not *required* to do so. Consequently floating grains are possible in this region of parameter space (lower-right region in Fig. 18). In our computer-generated packings we find significant fractions of floating grains only in this region, and in sufficient quantities to explain why anomalous density-velocity trends can occur. As VF increases, porosity and permeability both decrease rapidly.

CONCLUSIONS

Floating grains, *i.e.* grains that occupy volume but are not locked into a rigid load-bearing framework of grain-to-grain contacts, are postulated to explain anomalous trends of acoustic velocity vs. density and porosity. We find direct evidence of floating grains in a set of model sediments. The models are computer-generated, dense, disordered packings of spheres of two sizes, with prescribed ratios of sphere radii (RR) and volume

fractions (VF) of small spheres. In this work a grain is considered floating if it can be displaced 10% of its radius in at least one direction without encountering another grain.

Floating grains occur in all the packings. The volume fraction of floating grains is about 0.5% in monodisperse packings and in bidisperse packings with large volume fractions of small grains. The floating grain fraction can be larger by a factor of ten if two thresholds are met. First, VF must be smaller than 40%; otherwise the small grains must form part of the load-bearing framework. Second, the large grains must be at least three times larger than the small grains; otherwise the small grains cannot act as pore-filling and thus form part of the load-bearing framework. If these conditions are met, the small grains can fit into pore bodies formed by the large grains, but are not numerous enough to become “captured” into the load-bearing framework. These thresholds are analogous to phase transitions between three types of sediment structure: a matrix dominated by small grains with large grains as inclusions, a matrix dominated by large grains with small grains replacing some large grains, and a matrix dominated by large grains with small grains filling voids between large grains. The thresholds observed for floating grains are consistent with well established thresholds for porosity and permeability. Thus this work provides grain-scale insight that complements previously developed macroscopic models. An example is the variation in pore throat size distributions with VF and RR, predicted *a priori* from the computer-generated packings and quantitatively consistent with measurements of permeability.

Based on these results in a model system, we propose that floating grains will occur in poorly to semi-consolidated sediments if similar conditions on the grain size

distribution are met. The grain size distribution must be sufficiently broad for small grains to fit into the space between large grains that predominantly constitute the load-bearing framework in the sediment. The frequency of small grains must be large enough to represent a substantial volume of the sediment, but not so large that the contacts of small grains to small grains are a dominant part of the load-bearing framework. Predictions based on these conditions are quantitatively validated by several reservoirs in petroleum exploration province.

The occurrence of floating grains is a manifestation of "non-ideal" grain-scale packing. The velocity/density anomaly can therefore be related to other macroscopic properties that are influenced by non-ideal packing.

ACKNOWLEDGEMENTS

BHP Billiton supported this research and permitted its publication. Cynthia Thane developed the sphere packing code and performed most of the simulations reported here. She and SB were also supported in part by the US Dept. of Agriculture, grant NRI 2004-35102-14920. Prof. J. Finney kindly permitted access to his sphere location measurements. Dr. Maša Prodanović and Joanna Castillo provided expert assistance with the figures.

REFERENCES CITED

- Arns, C. H., F. Bauget, A. Ghouss, A. Sakellariou, T. J. Senden, A. P. Sheppard, R. M. Sok, W. V. Pinczewski, J. Kelly, and M. A. Knackstedt, "Digital core laboratory: Petrophysical analysis from 3D imaging of reservoir core fragments," *Petrophysics*, 46(4), 260-277, 2005.

- Bakke, S., Øren, P.E., 1997. 3-D pore-scale modeling of sandstones and flow simulations in the pore networks. *SPEJ* 2, 136–149.
- Bryant, S., Cade, C., and Mellor, D. "Permeability prediction from geologic models", *AAPG Bulletin*, (1993) 77 (8), 1338-1350.
- Bryant, S. and Raikes, S., "Prediction of Elastic Wave Velocities in Sandstones Using Structural Models," *Geophysics*, Vol. 60, No. 2, pp. 437-446, March - April 1995.
- Bryant, S., Mason, G., and Mellor, D., "Quantification of Spatial Correlation in Porous Media and Its Effect on Mercury Porosimetry," *Journal Colloid and Interface Science*, Vol. 177, pp.88-100, 1996.
- Clarke, R. Reservoir properties of conglomerates and conglomeratic sandstones. *AAPG Bull.* 63(5) 799-809, 1979.
- Clarke, A. and Wiley, J. Numerical simulation of the dense random packing of a binary mixture of hard spheres: Amorphous metals. *Phys. Rev. B*: 35(14) 7350-6, 1987.
- DeMartini, D. and Glinsky, M. "A model for variation of velocity versus density trends in porous sedimentary rocks," *J. Appl. Phys.* 100, 014910 (2006).
- Finney, J., Random packings and the structure of simple liquids. I. The geometry of random close packing, *Proceedings of the Royal Society of London. Series A. Mathematical, Physical and Engineering Sciences*, 319, 479-493, 1970.
- Furnas, C. "Flow of gases through beds of broken solids." *US Bur. Mines Bull.* 307, 144 (1929).
- Jin, G., Patzek, T.W., Silin, D.B., 2003. Physics-based reconstruction of sedimentary rocks. SPE Paper 83587. SPE Western Regional/AAPG Pacific Section Joint Meeting, Long Beach, CA, 19–24 May, 2003.

- Kamann, P., Ritzi, R., Dominic, D. and Conrad, C. "Porosity and Permeability and Sediment Mixtures." *Ground Water* 45(4):429-438 (2007).
- Kansal, A., Torquato, S. and Stillinger, F. "Diversity of order and densities in jammed hard-particle packings," *Physical Review E* 66, 041109 (2002)
- Koltermann, C.E. and S. M. Gorelick, "Fractional packing Model for Hydraulic Conductivity Derived from Sediment Mixtures", *Water Resources Research*, Vol. 31, No. 12 (1995): 3283-3297.
- Mason, G. and D. W. Mellor (1995). "Simulation of Drainage and Imbibition in a Random packing of Equal Spheres." *Journal of Colloid and interface Science* 176: 214-225.
- Mellor, D. "Random close packing of equal spheres; structure and implications for use as a model porous medium", PhD Thesis, Open University, Milton Keynes, 1989.
- Mousavi, M. and Bryant, S. "Geometric Models of Porosity Reduction Mechanisms in Tight Gas Sands," SPE 107963, 2007 SPE Rocky Mountain Oil & Gas Technology Symposium, Denver, Colorado, U.S.A., 16–18 April 2007.
- Øren, P.E., Bakke, S., Arntzen, O.J., 1998. Extending predictive capabilities to network models. *SPEJ* 3, 324–336.
- Park, N., Olson, J.E., and Holder, J., 2007, "The Application of Stress Corrosion Cracking to Time-Dependent Shale Stability", SPE Rocky Mountain Regional Meeting, Denver, CO.
- Park, N., Olson, J.E., Holder, J., and Rijken, P. DEM Analysis of Subcritical Growth: Effect of Diagenesis and Stress, *Golden Rocks*, 41st U.S. Symposium on Rock Mechanics, Golden, CO, (2006).
- Shakoor, A. and Cook, B. "The effect of stone content, size, and shape on the engineering properties of compacted silty clay." *Bull. Assoc. Eng. Geol.* 27(2):245-253 (1990).

Thane, C. “Geometry and Topology of Model Sediments and Their influence on Sediment Properties,” M.S. Thesis, Department of Petroleum and Geosystems Engineering, The University of Texas at Austin, 2006.

Thompson, K.E., C.S. Willson, and W. Zhang. “Quantitative computer reconstruction of particulate materials from microtomography images,” *Powder Technology* **163**:169-182 (2006).

Yerazunis, S., S. Cornell and B. Wintner. Dense random packing of binary mixtures of spheres. *Nature* **207**(4999): 835-7, 1965.

FIGURE CAPTIONS

Figure 1. One normal (reservoir I) and two anomalous (reservoirs II and III) trends of density vs compressional velocity in a petroleum exploration province. The dotted line shows the average trend for reservoirs in the region regressed from over 300 points covering a large portion of the basin (DeMartini and Glinsky, 2006). Uncertainty in the regression is indicated by the error bars (two standard deviations).

Figure 2 (Left) A regular packing of spheres has no floating grains. Each grain is locked in place by contacts with surrounding grains. No grain can move unless all other grains also move. (Right) Irregular packings, including dense, disordered packings, inevitably contain floating grains. The unshaded grain can move while the other grains remain fixed. The shaded grains have formed a rigid, load-bearing framework, so it is not easy to rearrange them. Thus the floating grain is likely to remain floating, even if the confining stresses on the sediment increase.

Figure 3. Grain-size distributions for the three reservoirs considered in Fig. 1. Reservoir I is relatively well sorted. Reservoirs II and III show a successively larger proportions of small grains to large grains. The hypothesis examined in this work is that the increasing fraction of small grains causes the velocity anomaly for Reservoirs II and III in Fig. 1.

Figure 4. Three steps of the cooperative rearrangement algorithm from left to right: (1) initial point generation, (2) sphere growth, and (3) overlap check and removal. The grains

indicated in the center panel undergo displacements so that they are in point contact, right panel. Steps (2) and (3) of the algorithm are iterated until a maximally dense packing is obtained. The packings are isotropic and do not account explicitly for any particular sedimentation process.

Figure 5. Example of model sediment created by the cooperative rearrangement algorithm in a periodic cubic domain. The porosity is 36%. This example contains about 100 spheres all the same size; packings used for analysis in this work contain 5000 spheres or more. The periodic boundaries allow spheres to extend beyond the nominal faces of the domain. This eliminates the introduction of local order in the packing by any smooth, confining wall.

Figure 6. Example test displacements for a floating grain. The displacement distance is exaggerated in the diagram. The results shown in this paper assumed a displacement of $0.1 R$ as the threshold for floating, R being the radius of test sphere.

Figure 7. Normalized Radial Distribution Function (RDF) of sphere centers for the Finney packing (dashed line) and a packing of equal spheres generated by the cooperative rearrangement algorithm (solid line) indicates that the algorithm creates packings with the same structural features found experimentally. The peak at $r = 2R$ corresponds to pairs of spheres in point contact; the plot truncates this peak so that other features are

visible. For example, the peaks at r_{AB} and r_{AC} correspond to spheres in the arrangements sketched.

Figure 8. Trends of porosity in dense, disordered bidisperse packings. Error bars show variation over ten or more realizations. As VF, the fraction of solid volume composed of small spheres, increases from zero, the porosity decreases to a minimum, then increases to the monodisperse limit of 0.36. As RR, the ratio of large sphere radius to small sphere radius, increases the minimum porosity decreases. The asymmetry of the trend of porosity vs VF for large RR is a manifestation of the transition from small spheres fitting into voids between large grains ($VF < 0.3$) to small spheres forming the matrix surrounding large grains ($VF > 0.4$).

Figure 9. (a) Predicted trends of porosity vs volume fraction of small spheres for two-size packings with $RR \leq 3$ are consistent with porosities measured in sphere packs, denoted YCW (Yerazunis et al, 1965), in broken solids, denoted Furnas (Furnas, 1929) and sand mixtures, denoted KRDC (Kamann et al., 2007). The predictions are also consistent with simulations of Clarke and Wiley (1987), denoted CW. Non-spherical grains (Furnas and KRDC) do not pack as densely as the spheres but the porosity trends are qualitatively similar. (b) Predictions for $RR > 3$ are consistent with porosities measured in broken solids, sand mixtures, sphere packs and clay/sand mixtures, denoted KG (Koltermann and Gorelick, 1995). The radius ratio for the clay/sand mixture is much larger than 10.

Figure 10. Cumulative frequency distribution of pore body sizes in Finney's dense disordered packing of equal spheres. Pore bodies are identified by Delaunay tessellation of the sphere centers. The body size r_b is taken to be the radius of the largest sphere that can be inscribed in the body. Radius is normalized by sphere size R . Small spheres that are half the size of the Finney spheres ($RR = 2$) could be placed in only in the largest 10% of the pores. Thus small spheres in bidisperse packings with $RR = 2$ or less tend to be framework grains, occupying the same positions that a large sphere would in a monodisperse packing. In contrast, small spheres that are a third the size of the Finney spheres ($RR = 3$) will fit in all but the smallest 30% of the pores. In a bidisperse packing with $RR = 3$ or greater, the small spheres tend to be pore-filling grains, occupying voids within a framework of large spheres. This increases the occurrence of floating grains.

Figure 11. 2D slices from two-size packings with ranges of values of RR and VF . The porosity of each packing is given in the upper-right corner of each slice.

Figure 12: Pore throat size distributions obtained analytically from dense, disordered, bidisperse packings. In each plot the pore throat size distribution of a monodisperse packing is plotted as a dashed line for reference. The increase in small throats and concomitant decrease in large throats is pronounced as VF increases from zero and as RR increases. Beyond a threshold of $VF = 0.4$, however, the distributions change relatively little.

Figure 13: Effect of displacement distance on the volume percent of floating grains found in monodisperse computer-generated packings (top) on linear scale and (bottom) on logarithmic scale.

Figure 14: Volume percent of floating grains in packings of RR 1.5, 2, 3 and 4. A grain is considered floating if it can move a distance equal to 10% of its radius without encountering another grain. The maximum occurs when there are sufficient numbers of sufficiently small grains to fit into the voids between larger grains forming the load-bearing framework. If too many small grains are present (40% volume fraction is the threshold), they become part of the framework. If the small grains are too large to fit into the voids (RR = 2 is the threshold), they become part of the framework.

Figure 15: A pore defined by four large grains taken from a bidisperse packing with VF = 40%, RR=5. The small grains pack tightly into a pore body between large grains, and both large and small grains are part of the load-bearing framework.

Figure 16: Porosity of a two-size packing of spheres is only a weak indicator of the volume fraction of floating grains. Floating grains occur much more often when the grain size distribution satisfies two conditions, $RR > 3$ and $VF < 0.40$. Those characteristics lead to lower porosities, but other characteristics can also reduce sediment porosity without satisfying the conditions for the occurrence of floating grains.

Figure 17: The fraction of small spheres that are captured, i.e., that form part of the load-bearing framework, increases with volume fraction of small spheres. At a given value of VF, the capture fraction increases as the radius ratio (RR) decreases. Above the threshold $VF_c = 40\%$, nearly all the small grains are part of the load bearing framework.

Figure 18: Characteristic features of bidisperse packings can be thought of in terms of phase transitions with the parameter space [RR, VF]. In particular, floating grains only occur below a threshold value of VF and above a threshold value of RR (lower right part of the domain). For sediments that satisfy both thresholds there will be a significant fraction of floating grains. This will lead to a relatively incompetent rock that will have significantly lower compressional velocity than would be expected for an equivalent well sorted rock of the same porosity. This lack of sorting also leads to significantly smaller pore throats and a correspondingly lower permeability.

FIGURES
(Included for reference purposes.)

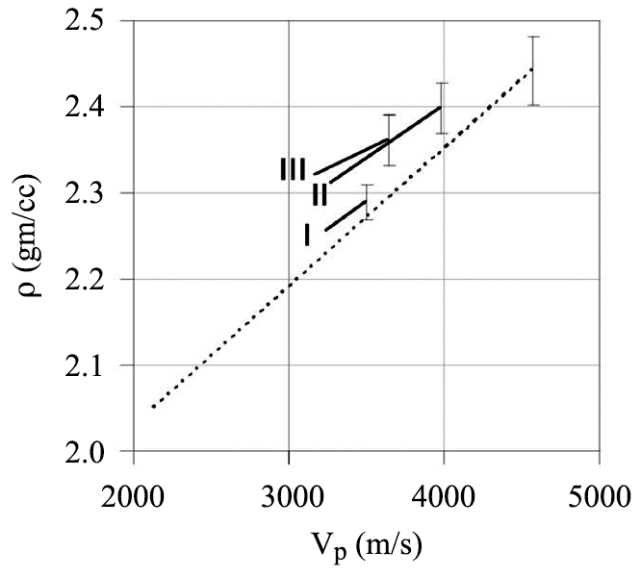


Figure 1.

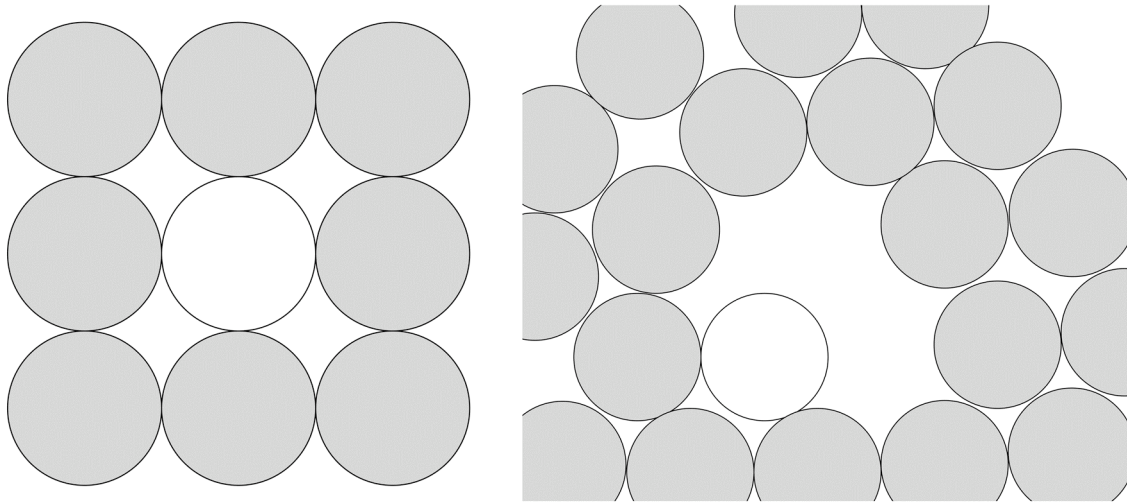


Figure 2.

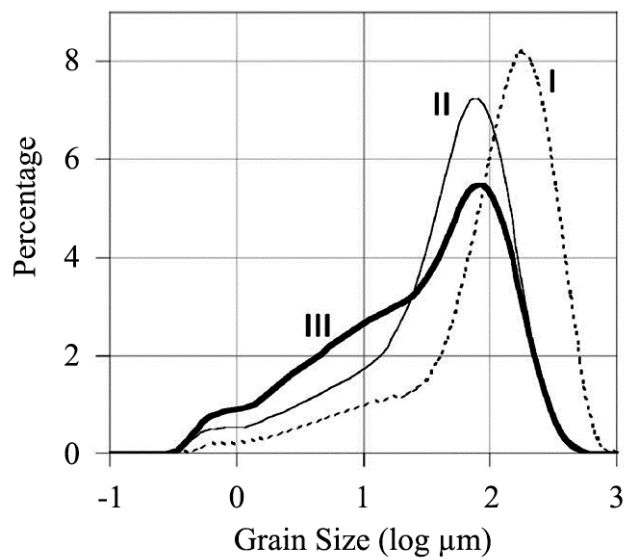


Figure 3.

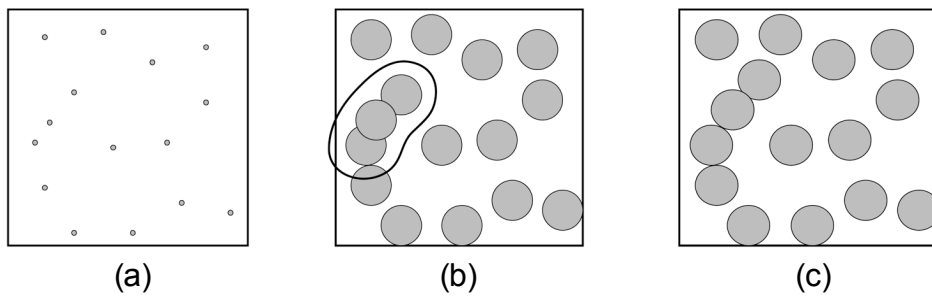


Figure 4

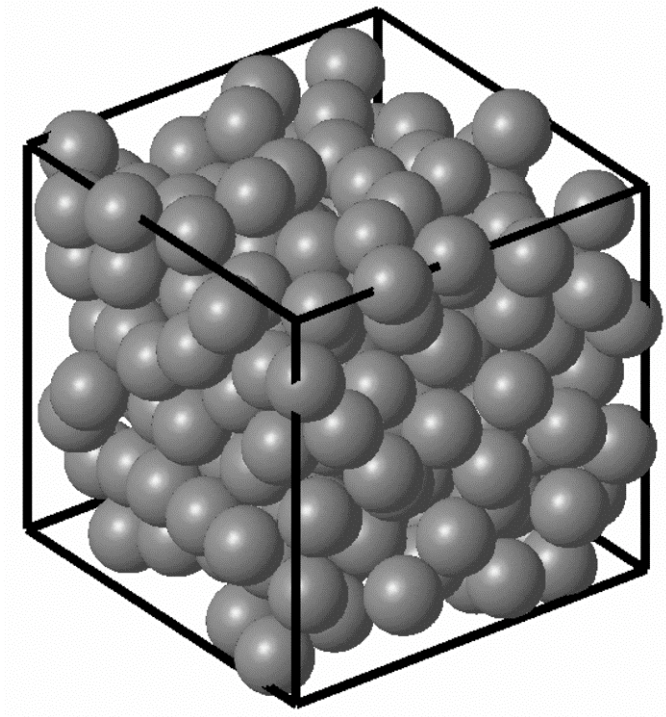


Figure 5.

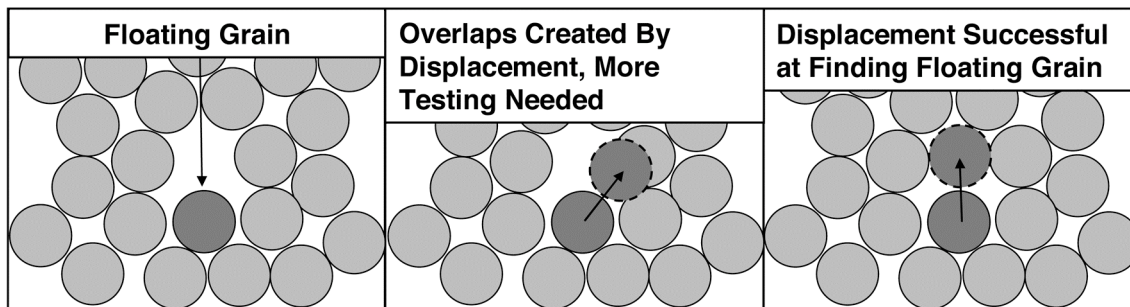


Figure 6:

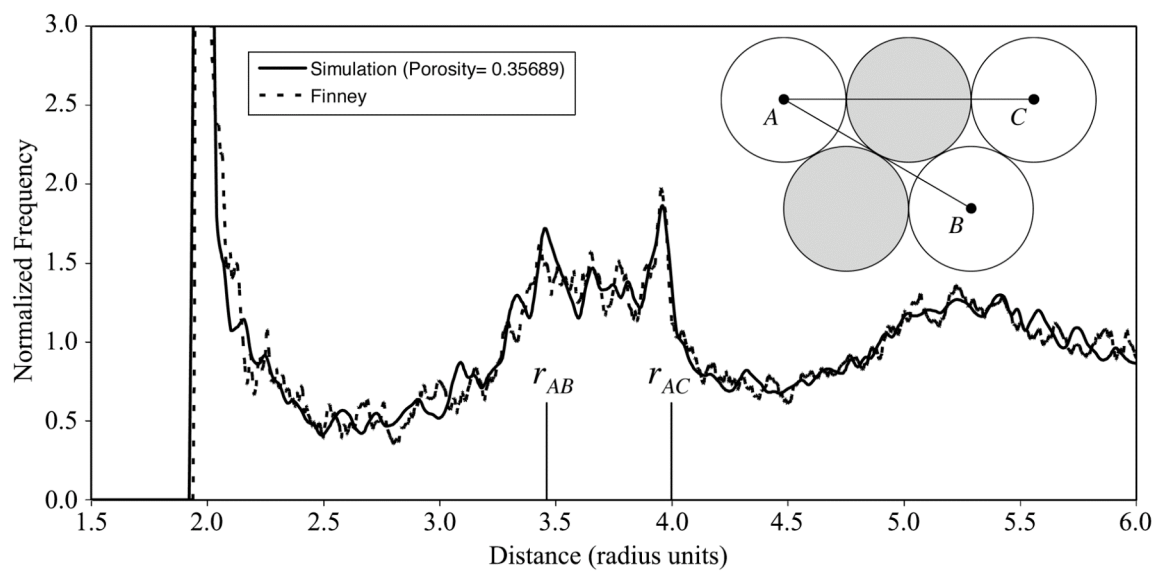


Figure 7

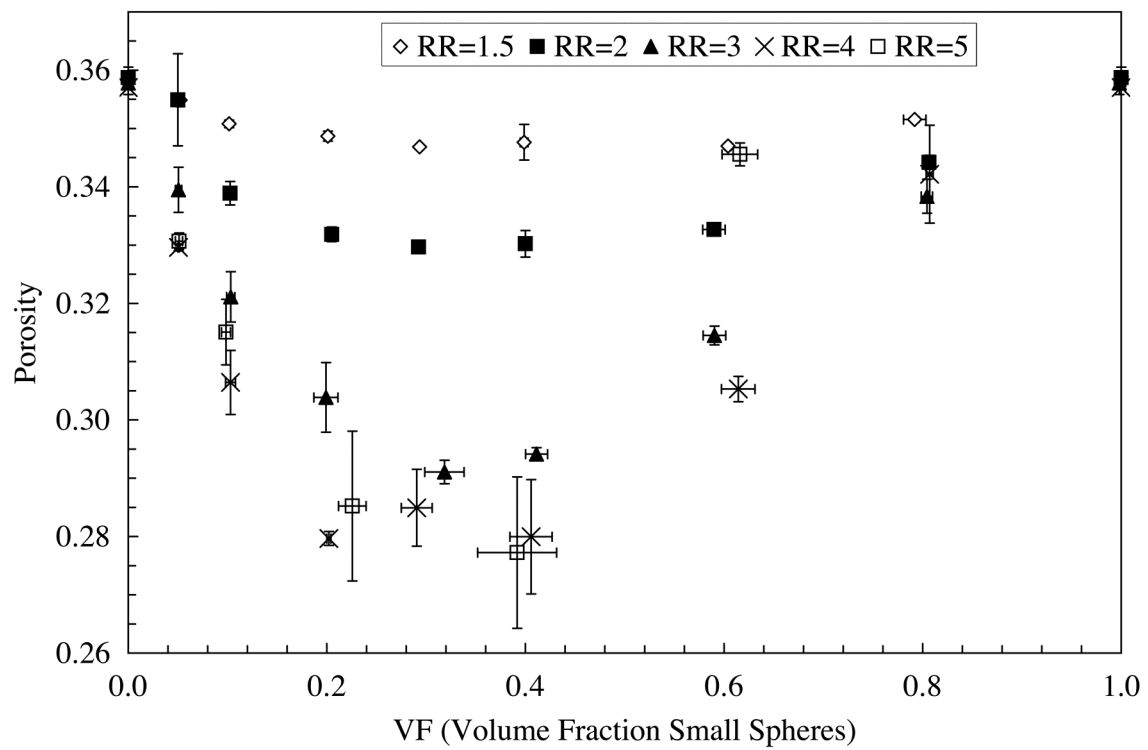


Figure 8.

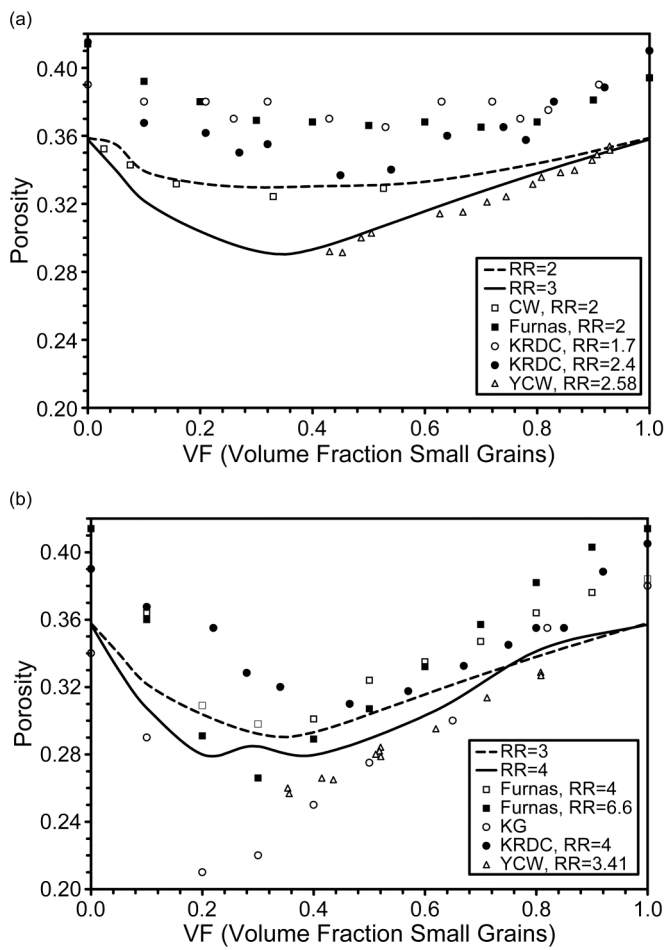


Figure 9.

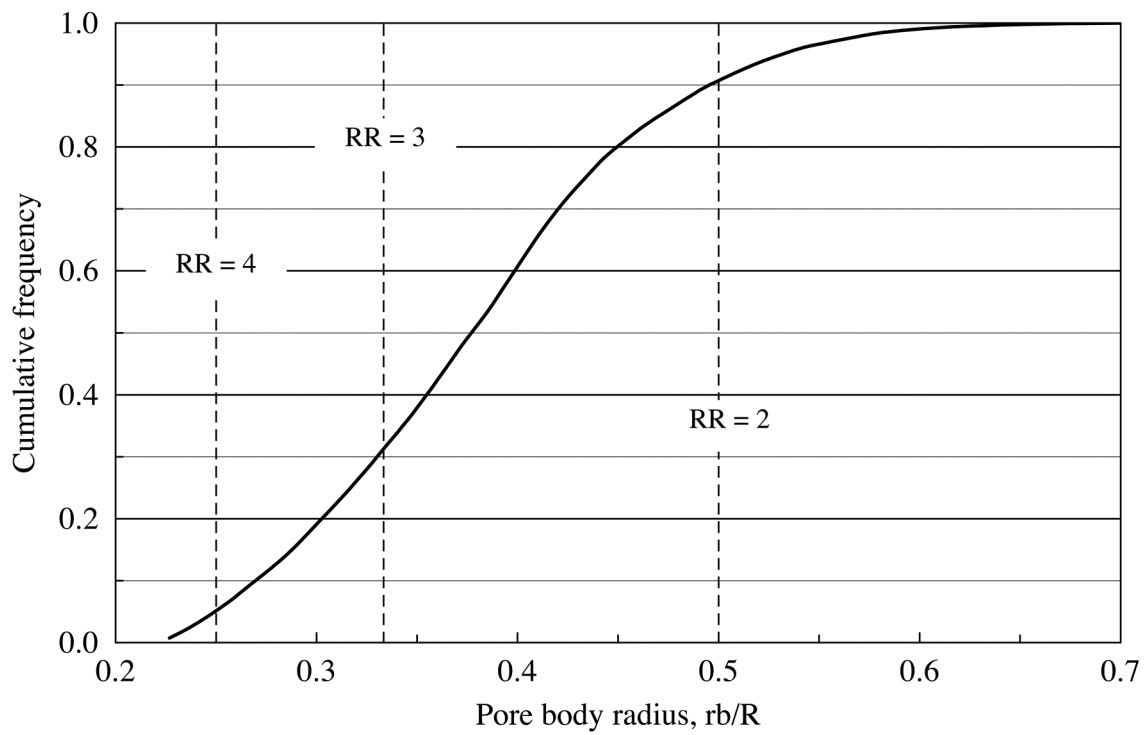


Figure 10.

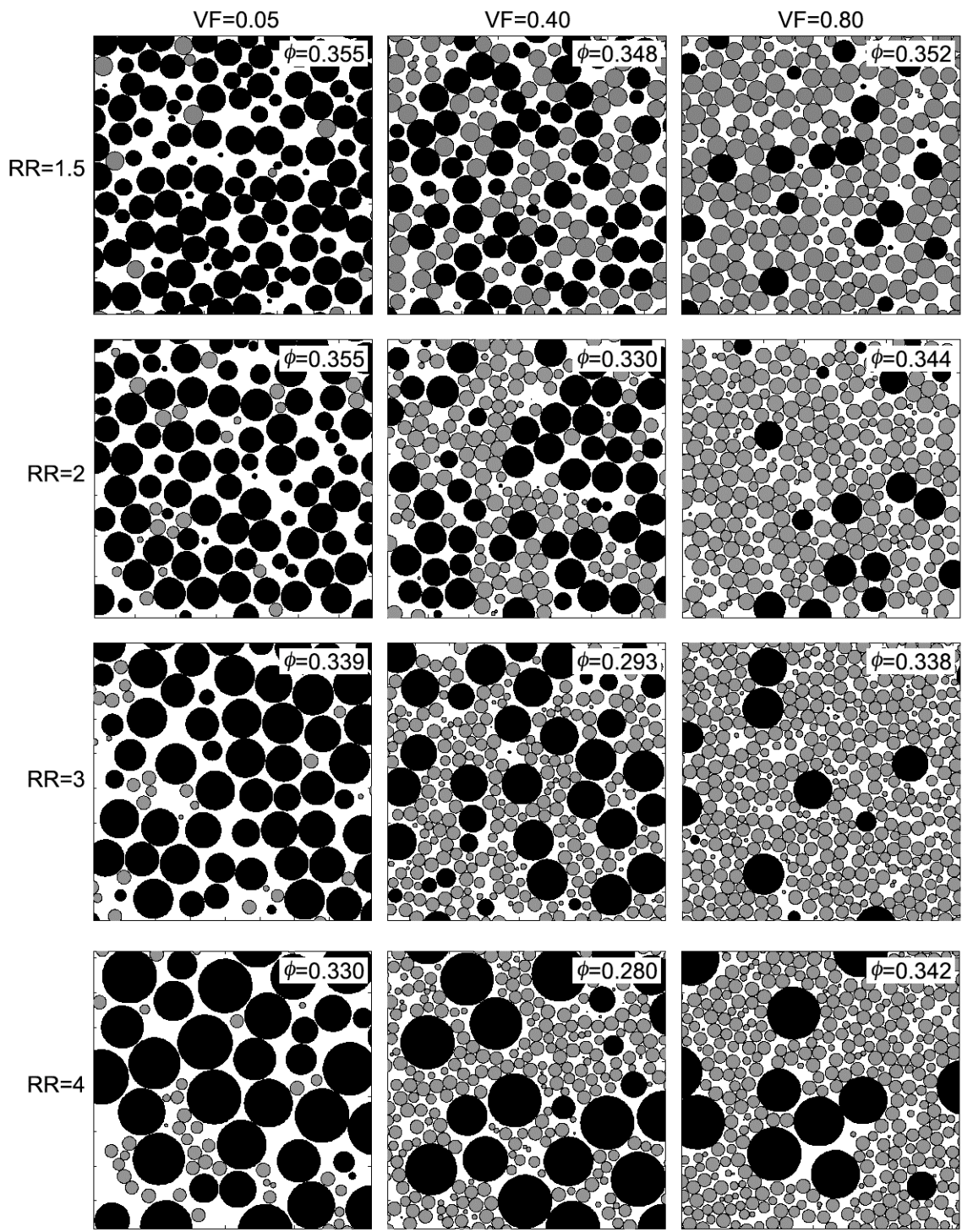


Figure 11

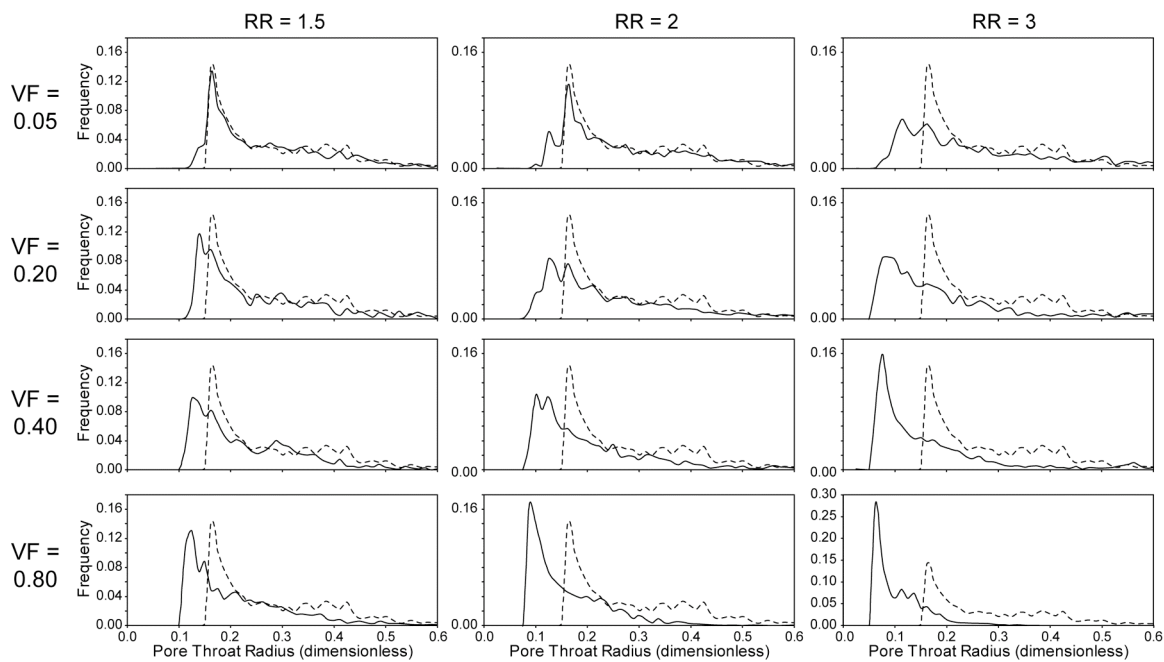


Figure 12:

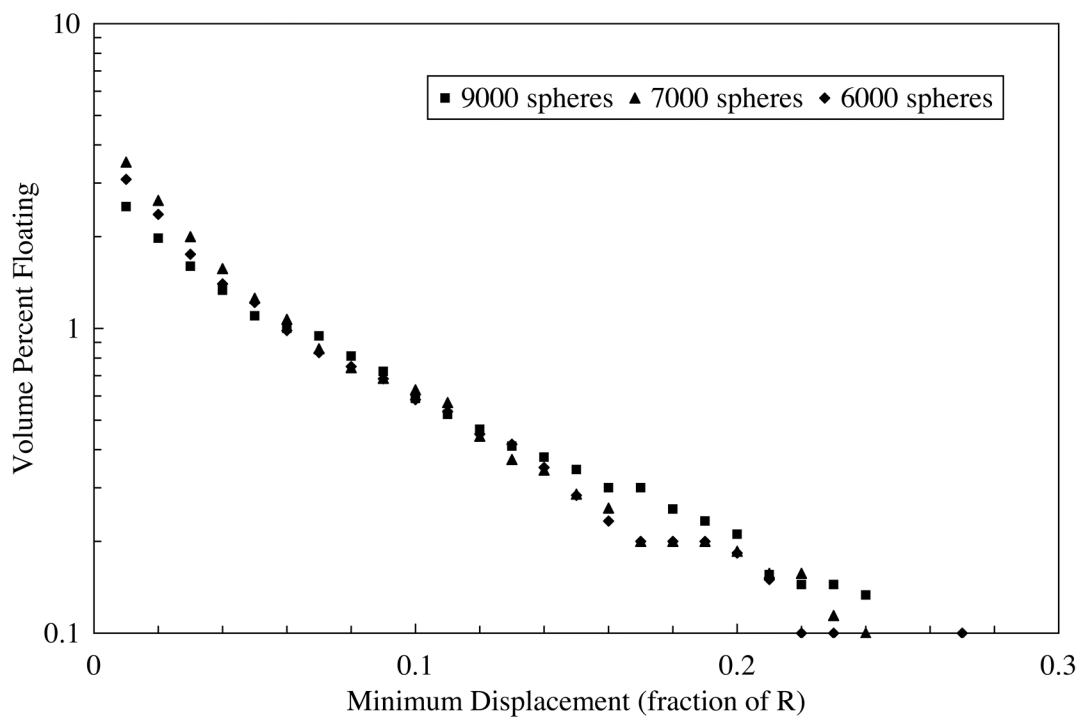
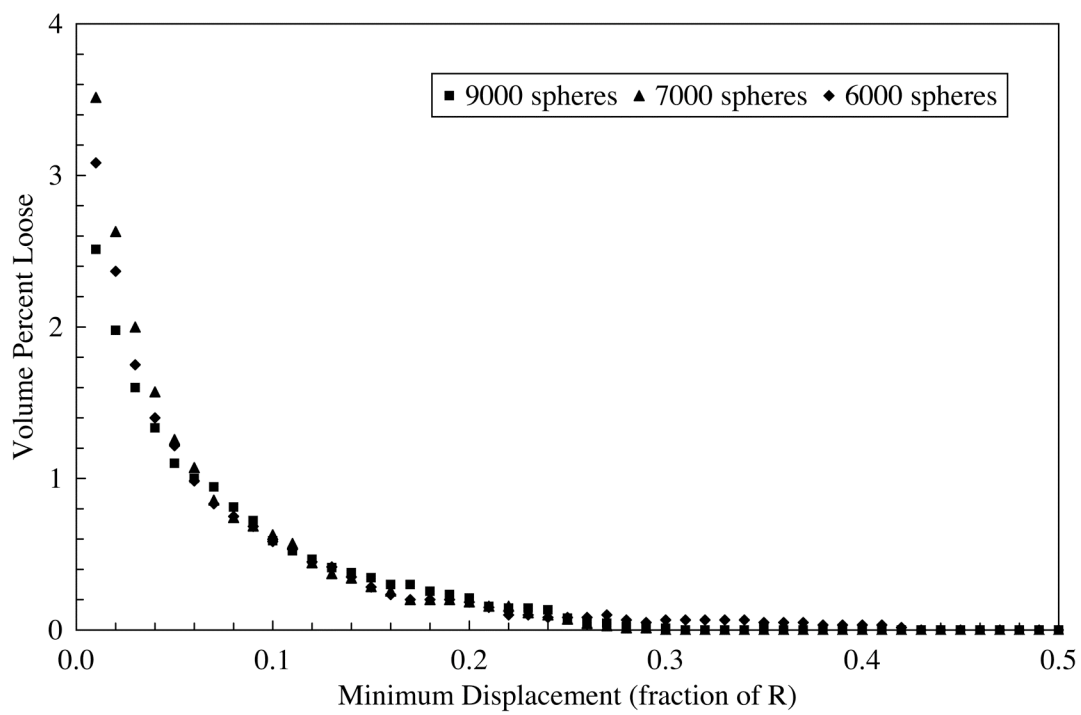


Figure 13:

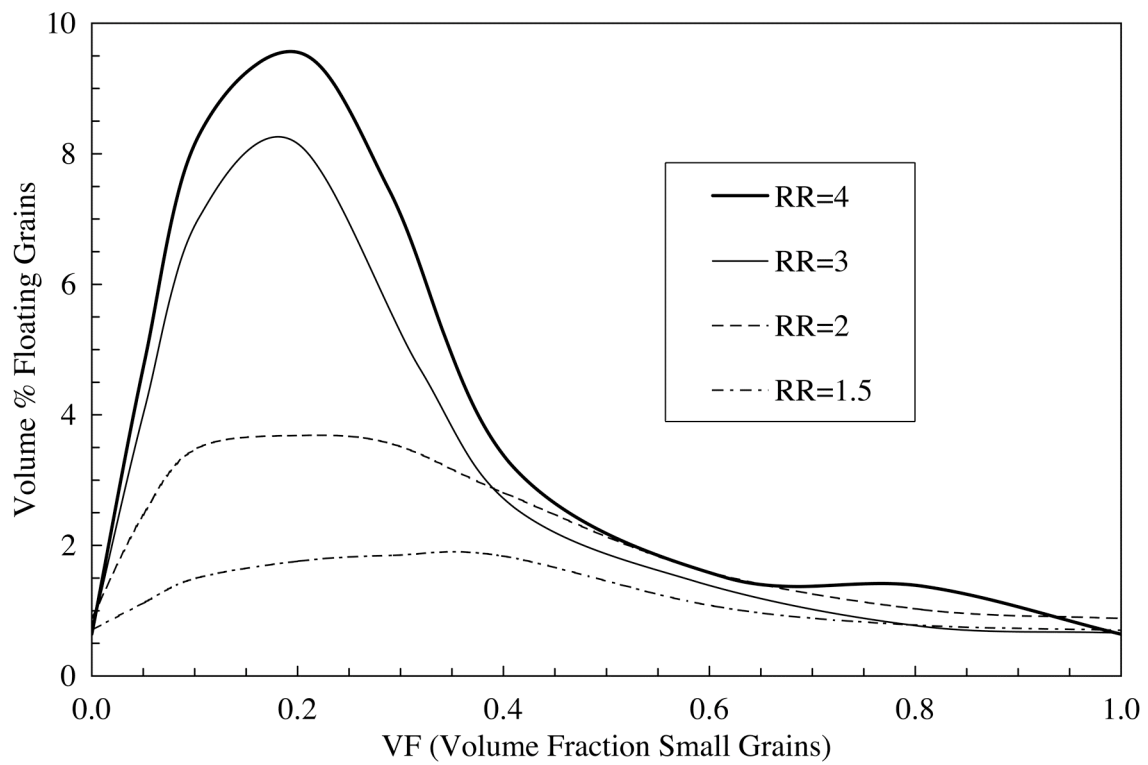


Figure 14

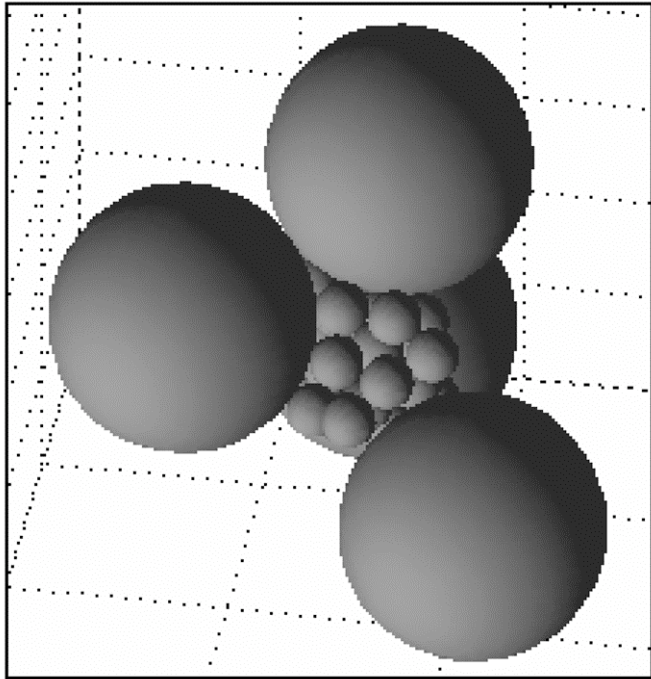


Figure 15:

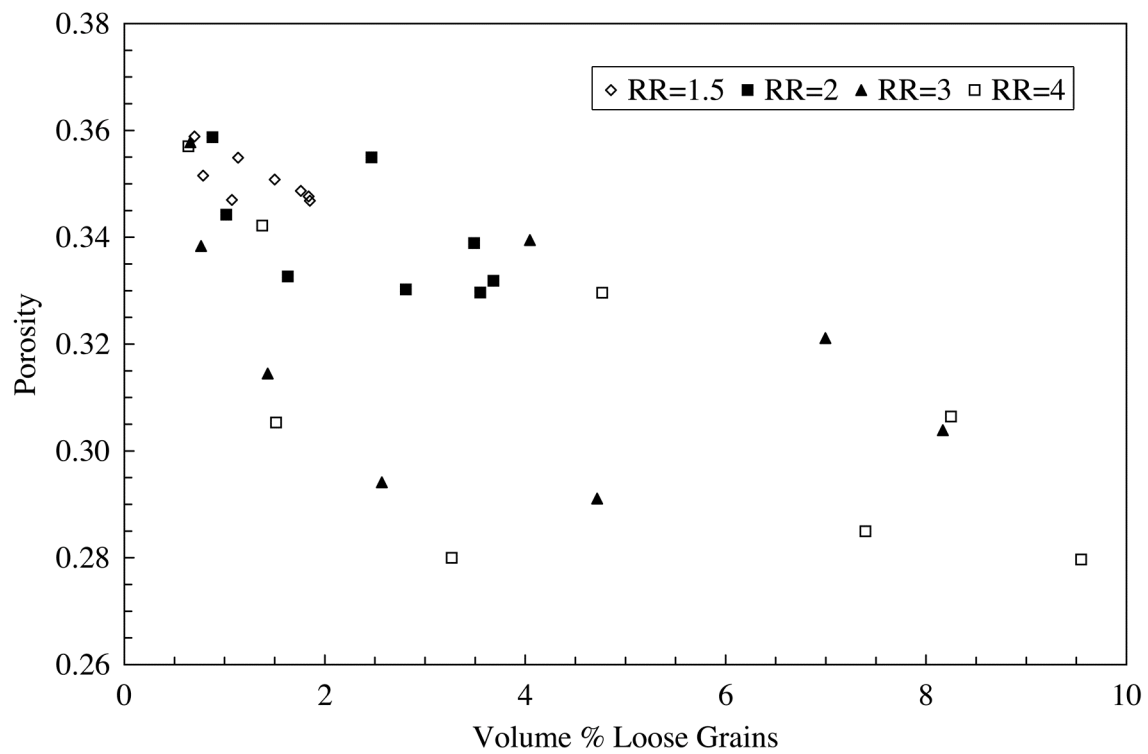


Figure 16

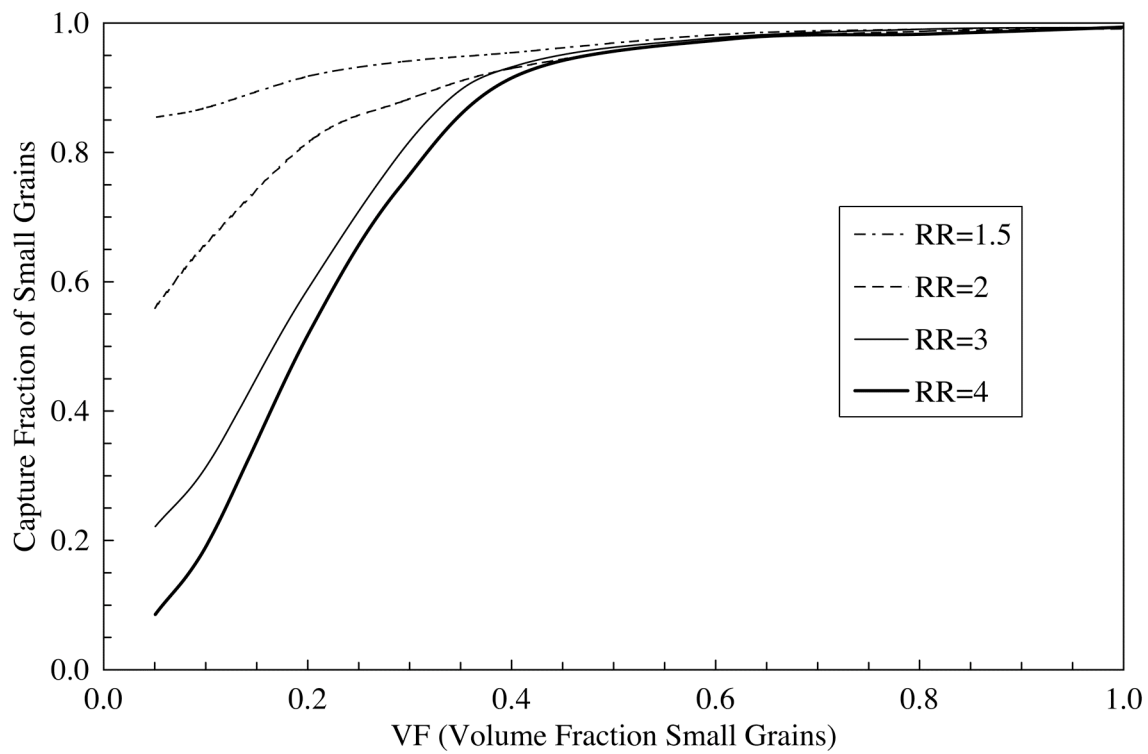


Figure 17:

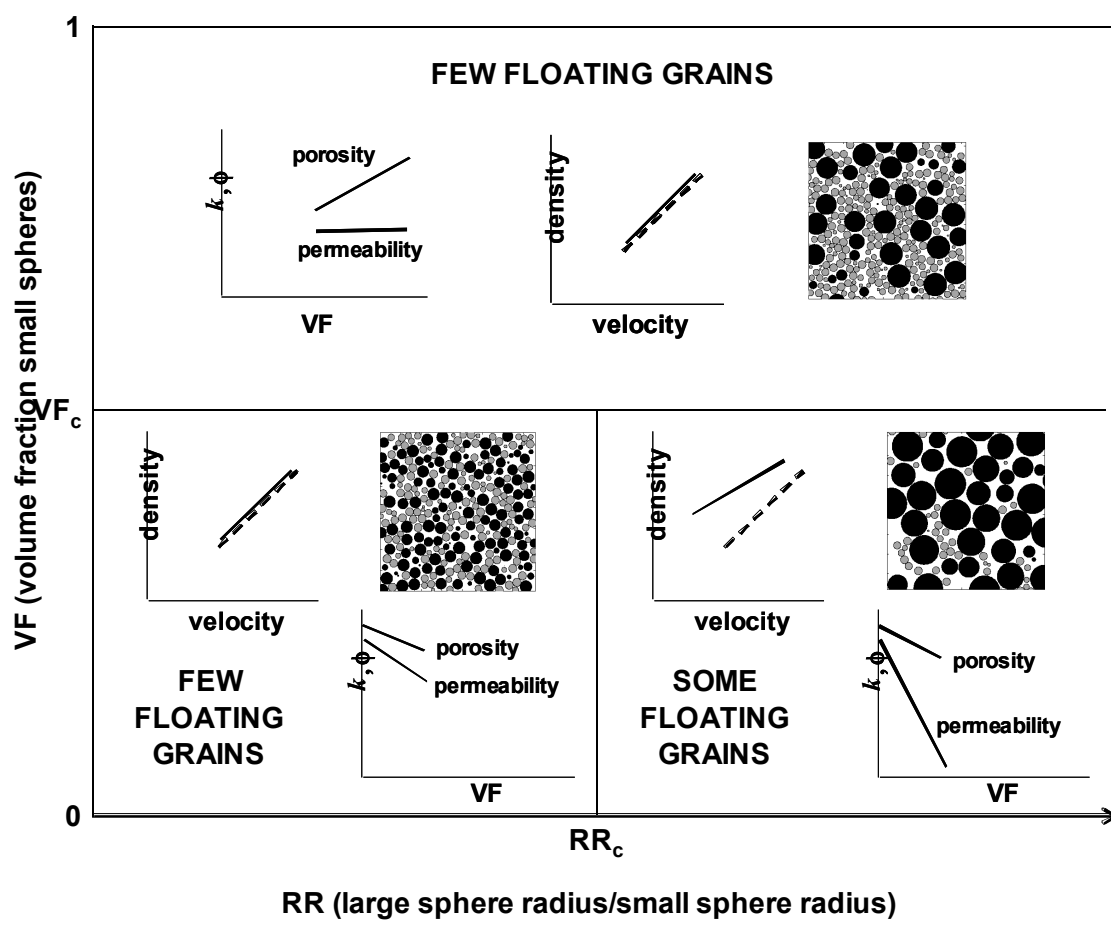


Figure 18: